MCWASP 2006 Nice France *Edited by*
TMS (The Minerals, Metals & Materials Society), Year

A POROSITY MODEL FOR MULTI-GAS SYSTEMS IN MULTI-COMPONENT ALLOYS

G. Couturier[(1,2)], J.-L. Desbiolles[(1,2)], M. Rappaz[(1)]

[(1)] Computational Materials Laboratory, School of Engineering,
Ecole Polytechnique Fédérale de Lausanne, Station 12, CH-1015 Lausanne, Switzerland
[(2)] Calcom ESI, PSE-A, CH-1015 Lausanne, Switzerland

Keywords: porosity, gas microsegregation, pressure drop, gas thermodynamics.

Abstract

A general framework for the modelling of porosity formation in multi-component alloys with more than one gaseous element is considered in the present contribution. It offers several advantages and accounts for: i) the partial pressure of any gaseous element composed of one or two chemical elements (e.g., H_2, N_2, CO, etc.); ii) the influence of the alloy composition on partial pressures through chemical activities; iii) the account of both trace gaseous elements and volatile solute elements such as zinc through appropriate mass balances. The set of equations describing multi-gas equilibrium at a given location is first described, with the construction of appropriate databases for aluminium-, copper- and iron-base alloys. These local state equations are coupled to a macroscopic resolution of the Darcy-mass balance equations governing the pressure drop in the mushy zone. This solution is based on an evolving fine volume grid superimposed to a finite element mesh used for the heat flow computations [1]. A few applications illustrate the effects of process and alloy parameters on the final porosity fraction.

Introduction

Porosity in castings is a major defect since it affects the mechanical properties [2-6], in particular the initiation of fatigue cracks [2-4]. Therefore, the reduction of porosity fraction and size, the control of porosity distribution and morphology are crucial for the optimization of fatigue behaviour of as-cast components. Porosity is the result of two concomitant mechanisms: (i) solidification shrinkage induces a suction and thus a liquid pressure drop in the mushy zone (Darcy's law [7]), (ii) trace gaseous elements in the liquid being generally less soluble in the solid phase, solidification induces gas microsegregation in the remaining liquid part. Cavitation may occur in the mushy zone when the effective gas concentration in the liquid, w_g^l, reaches the gas solubility, w_g^{l*}. The solubility furthermore decreases with liquid pressure and temperature.

In aluminium-base alloys, hydrogen is the only diatomic gas enough soluble to lead to porosity formation [8-10]. Hydrogen in aluminium alloys is due to air moisture decomposition ($H_2O \rightarrow 2H+O$) and aluminium oxidation [11] ($3H_2O+2Al \rightarrow Al_2O_3+3H_2$) and is also produced by the decomposition of moisture or grease covering tools immersed into the melt. In copper-base alloys, hydrogen, moisture, and sulphur dioxide are responsible of porosity formation [12], whereas this defect is due to hydrogen, nitrogen and carbon monoxide in iron-base alloys [13]. The combined effects of hydrogen and nitrogen in steel has already been studied [14,15]. Carbon solubility in copper-base alloys seems to be too low to form carbon monoxide [10]. As the affinity of the reaction of formation of FeO is higher than that of SO_2 [16], SO_2 is never formed

in iron-base alloys. Some volatile solute elements (e.g., zinc) can also contribute to microporosity [17]. Several authors reported the effect of alloying elements on gas solubility in aluminium-, copper-, and iron-base alloys [11, 12, 14, 16].

The general framework of the present contribution is the formation of porosity in the presence of one or more gases, the solubility of which being dependent on several alloying elements. The basic conservation and thermodynamics equilibrium equations that govern porosity formation in the case of a multi-gas system in multi-component alloys are established in the first part. A realistic growth law for a pore constrained by the dendrite network is proposed in the second part. In the final part, this multi-gas approach is applied to the case of porosity formation in copper-base alloys. The impact on porosity fraction of the presence of H, S and O in solution in the alloy is studied for various solidification conditions.

Multi-Gas and Multi-Component Approach

The purpose of this part is not to describe again the equations that govern porosity formation in the case of one diatomic gas, g, (e.g., H_2 in an aluminium-base alloy). These equations have been largely explained in previous papers [1,17]. In this part, a method for the extension of the approach to several gases composed of one or two chemical elements soluble in a multi-component alloy is proposed.

Gas Thermodynamics

The gases responsible of porosity formation are generally composed of one or two chemical elements that can be solute elements of the alloy or not (see introduction). While Sievert's law applies to diatomic gases, the more general case of a gas composed of one or several elements is handled through solubility products. The involved reactions for gases made of maximum two elements are:

$$\text{Formation of gas } \alpha\ (\alpha = 1, n_g): \quad n_A^\alpha A \text{ or } n_A^\alpha A + n_B^\alpha B \leftrightarrow \alpha \text{ with } \alpha = A_{n_A^\alpha} \text{ or } A_{n_A^\alpha} B_{n_B^\alpha} \quad (1)$$

There are n_g gases contained in the gaseous phase and n_s chemical elements involved in the formation of these gases (represented by capital letters). n_A^α indicates the stoechiometry of the element A in gas α (e.g., 2 for H in H_2). On the left hand side of these reactions, the elements are dissolved in the liquid phase. The solubility product for gas α formed from A and B elements is recalled here:

$$\frac{p_\alpha / p_0}{\left(f_A^l X_A^{l*}\right)^{n_A^\alpha} \left(f_B^l X_B^{l*}\right)^{n_B^\alpha}} = \exp\left(\frac{-\Delta G_\alpha^0}{RT}\right) = K_\alpha(T) \quad (2)$$

p_α is the partial pressure of gas α, $\Delta G_\alpha^0(T)$ the variation of the standard Gibbs free energy for the reaction of formation of gas α, $K_\alpha(T)$ is the "constant" of the gas α formation reaction, f_A^l and f_B^l are the activity coefficients of elements A and B, and X_A^{l*} and X_B^{l*} the molar fractions in the liquid phase of elements A and B, respectively, in equilibrium with the gas phase. The Gibbs free energy variation, $\Delta G_\alpha^0(T)$, can be expressed as a function of the standard enthalpy, $\Delta H_\alpha^0(T)$, and the standard entropy $\Delta S_\alpha^0(T)$ (usually assumed constant in the temperature range):

$$\Delta G_\alpha^0(T) = \Delta H_\alpha^0(T) - T\Delta S_\alpha^0(T) \quad (3)$$

Eq. (2) can be transformed into the following relation:

$$\frac{p_\alpha / p_0}{\left({}^{'}f_A^l X_A^{l*}\right)^{n_A^\alpha}\left({}^{'}f_B^l X_B^{l*}\right)^{n_B^\alpha}} = A_\alpha \exp\left(-\frac{\Delta H_\alpha^0}{RT}\right) = {}^{'}K_\alpha(T) \qquad (4)$$

$$\text{with} \quad A_\alpha = \left({}^{*}f_A^l\right)^{n_A^\alpha}\left({}^{*}f_B^l\right)^{n_B^\alpha} \exp\left(\frac{\Delta S_\alpha^0}{R}\right) \quad \text{and} \quad {}^{'}f_A^l = \frac{f_A^l}{{}^{*}f_A^l}.$$

The activity coefficient of A, ${}^{*}f_A^l$, corresponding to the pure liquid metal, it follows that ${}^{'}f_A^l$ is equal to 1 in the absence of solute elements. The parameter A_α has no physical meaning but will be called the gas formation coefficient.

Similar expressions to relation (4) are obtained for other gases, and these expressions are the first n_g dependency relations proposed between the (n_g + n_s) unknown variables X_A^{l*} (A = 1, n_s), p_α (α = 1, n_g). The activity coefficient ratio ${}^{'}f_A^l$ is given by the following relationship [11]:

$${}^{'}f_A^l = 10^{\left(\sum_S e_A^S c_S + r_A^S c_S^2\right)} \qquad (5)$$

where e_A^S and r_A^S are the first- and second-order interaction coefficients of the solute element S on the gaseous element A, respectively. In this relation, the solute element concentrations, c_s, are expressed in wt%. Interaction coefficients for several solute elements in various alloys (Al, Cu, Fe,…), as well as ΔH_α^0 and A_α can be found in the literature [11,12,14,16,18].

A simple thermodynamic analysis [17] has shown that solute elements with a high vapour pressure (e.g., zinc) can contribute to the increase of the pore fraction in high melting point alloys (e.g., copper-base alloys). Relation (4) is also perfectly adapted to describe the transformation of such solute elements into a vapour phase.

Gaseous Element Conservations

The gas element conservation equation established in reference [17] for a diatomic gas in the presence of porosity can be easily extended to a multi-gas system. For each element A, one has:

$$\langle\rho\rangle X_{Ao}^l = \rho_l (1 - g_s) X_A^{l*} + \rho_s g_s k_A X_A^{l*} + M_{alloy}^o \frac{g_p}{RT} \sum_{g \ni A} n_A^g p_g \qquad (6)$$

where X_{Ao}^l and X_A^{l*} are the nominal molar concentration and the solubility limit in the liquid phase, respectively, and k_A is the partition coefficient of gaseous element A. ρ_l and ρ_s are the specific masses of the liquid and solid, respectively, while $\langle\rho\rangle$ is the average specific mass of the solid-liquid mixture in the absence of porosity. g_s and g_p are the volume fractions of solid and porosity, respectively, M_{alloy}^o is the molar mass of the alloy in the initial state (before solidification), T is the temperature and R the perfect gas constant. In this equation, the summation of the gas partial pressures is carried out for all the gases containing element A, with a weight given by the stoechiometry of element A in each gas.

In the presence of porosity, Eqs (6) provide n_s additional relationships between the unknown variables X_A^{l*}, X_B^{l*}, ..., X_N^{l*}, p_α, ..., p_λ and g_p. Therefore, Eqs (4) and (6) provide n_g+n_s relations in which n_g+n_s+1 unknown variables are present, i.e., one equation is still missing.

In the absence of porosity, relation (6) becomes:

$$X_A^l = \frac{\langle \rho \rangle X_{Ao}^l}{\rho_l (1 - g_s) + \rho_s g_s k_A} \tag{7}$$

Mechanical Equilibrium of a Pore

An additional equation is provided by the mechanical equilibrium condition of a pore:

$$p_p = p_\alpha + ... + p_\lambda = p_l + \Delta p_r \tag{8}$$

where p_p and p_l are the pressures in the pore and in the surrounding liquid , respectively, while Δp_r is the Laplace contribution associated with the curvature of the pore:

$$\Delta p_r = \frac{2\gamma_{gl}}{r} \tag{9}$$

where γ_{gl} is the surface energy of the pore/liquid interface and r the radius of curvature of the pore. Relation (8) introduces two unknown variables, p_l and r (i.e., n_g+n_s+3 unknowns with n_g+n_s+1 equations), but two more equations are provided by:

- The mass conservation equation coupled with Darcy's law that relates the liquid pressure with the porosity fraction. This relation has been largely detailed in previous papers [1,17] and will not be repeated here.
- A relationship between g_p and r. For a spherical pore, this relationship is straightforward, while a simple model for a pore constrained to grow within a dendritic network is developed in the next section.

In order for a pore to nucleate in the liquid, its initial radius of curvature, r_o, must satisfy Eq. (9), i.e., the supersaturation, $p_\alpha + \ldots + p_\lambda - p_l$, must be equal to the Laplace contribution.

Solution

The mass conservation equation coupled with Darcy's law is solved using an evolving fine volume grid superimposed to a finite element mesh used for the heat flow computations [1]. The set of n_g+n_s+2 equations governing at a local scale the relationship $g_p(p_l)$ in a multi-gas system is strongly non linear. In order to limit the computation time, these equations are solved for each grid of the mesh by one step of Newton-Raphton's method. This is equivalent to deriving Eqs (4), (6) and (8) in order to obtain a linear system with respect to dX_A^{l*}, dX_B^{l*}, ..., dp_α, dp_β..., dp_l and dg_p.

Growth Law

As the interface energy, γ_{gl}, is on the order of 1 Jm^{-2} and the pore curvature radius is equal to a few tens of micrometers, the curvature contribution (Laplace's overpressure, Eq. (9)) cannot be neglected in Eq. (8) and strongly influences the pore fraction. While the relationship between g_p and r is straightforward for spherical pores (i.e., gas porosity), a simple model for the curvature of a pore constrained to grow in a well developed dendritic network (i.e, shrinkage porosity) is derived in this section.

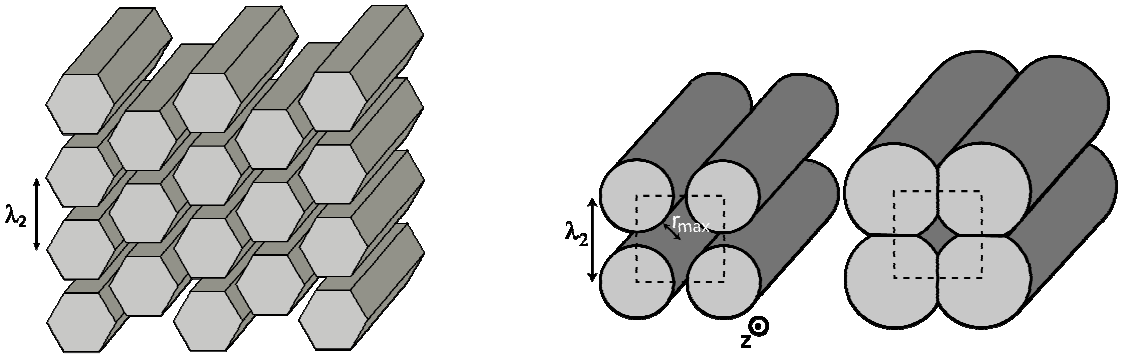

Figure 1. Regular stacking of dendrite arms, showing the space available for pores (r_{max}): hexagonal arms without impingement (left), and cylindrical arms with impingement (right).

The left scheme of Fig. 1 is an illustration of a too simple geometrical solution that does not take into account secondary dendrite arms impingement. The present model considers a simplified 3-dimensional network of cylindrical secondary dendrite arms and takes into account their impingement (right scheme in Fig. 1). Assuming that pores can grow in between the cylindrical arms, assumed to be infinite in length, the maximum radius of the pore is simply given by:

$$\text{if } g_s \le \frac{\pi}{4} \text{ (i.e. before impingement), } r_{max} = \frac{\lambda_2}{2}\left(\sqrt{2} - \left(\frac{g_s}{\pi}\right)^{1/2}\right) \tag{10}$$

$$\text{else, } \quad g_s = 2\left(\frac{1}{4} - \sqrt{2}\frac{r_{max}}{\lambda_2} + \left(\frac{r_{max}}{\lambda_2}\right)^2\right)^{1/2} + 4\left(\frac{\pi}{4} - \arccos\left(\frac{1}{\sqrt{2} - 2\frac{r_{max}}{\lambda_2}}\right)\right)\left(\frac{1}{\sqrt{2}} - \frac{r_{max}}{\lambda_2}\right)^2 .$$

As the liquid phase is assumed to completely wet the solid, the contact angle at the triple point (pore-solid-liquid) is zero. The relationship given by Eq. (10) is shown in Fig. 2, together with another relation, $r_{max} = 0.5\,\lambda_2(1 - g_s^{0.5})$, that corresponds to the solution of the left geometry in Fig. 1. It appears that the new relation (14) seems more adapted to the modelling of shrinkage porosity. Indeed, with $r_{max} = 0.5\,\lambda_2(1 - g_s^{0.5})$, r_{max}/λ_2 does not exceed 0.025 for $g_s \ge 0.9$. Taking λ_2 = 40 μm, r_{max} will be smaller than 1 μm, and Δp_r will be greater than 1.8 MPa. Therefore, pores will have almost no chance to grow if they do not nucleate before g_s = 0.9. Doing the same calculation with Eq. (10) ($r_{max}/\lambda_2 < 0.15$ for $g_s > 0.9$), the curvature contribution is on the order of 300 kPa during the last stage solidification, thus allowing shrinkage porosity formation. Eq. (10) will be retained for the simulations presented in the last part.

Results

The present porosity model has been applied to brass alloys, more specifically to a Cu-10%wtZn alloy. For the solidification path, the Scheil-Gulliver microsegregation model was used. The solidification range was assumed equal to 43 °C (no peritectic reaction was considered). The resolution of Darcy+mass balance equations is possible if solidification shrinkage is known [1]: the liquid and solid specific masses were assumed constant and equal to 7940 and 8960 kg/m^3, respectively.

In order to speed up the computations, an ideal one-dimensional directional casting was chosen. The casting velocity, v, and the thermal gradient, G, were equal to 0.01 m/s and

500 °C/m, respectively. The simulation results deal with the porosity fraction for the stationary regime, showing the impact of hydrogen, moisture and sulphur dioxide on porosity fraction.

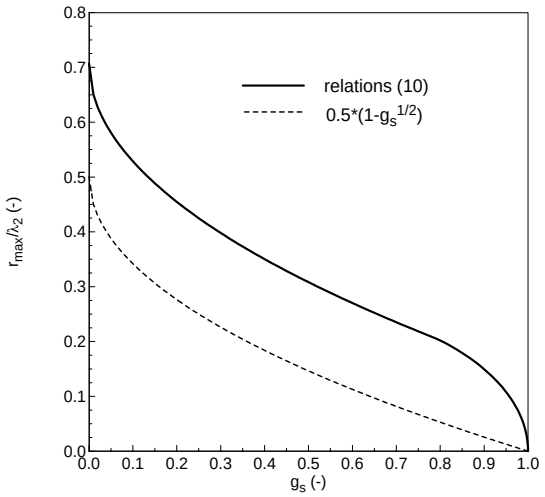

Figure 2. Representation of the maximum radius of a pore (normalized by the secondary dendrite arm spacing) growing in a mushy zone for the two geometrical models shown in Fig. 1.

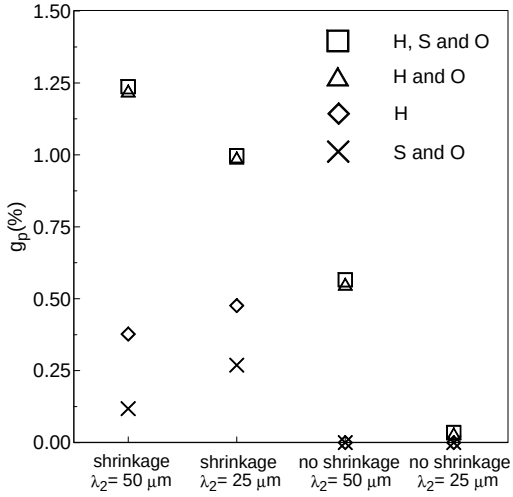

Figure 3. Porosity fraction in Cu-10 wt%Zn for different gaseous element systems (X^l_{Ho} = 30 ppm (at) , X^l_{So} = 0.8 % (at) and X^l_{Oo} = 20 ppm (at) if present). Two secondary dendrite arm spacings were tested, without and with account of solidification shrinkage.

In Fig. 3, the contribution to porosity formation of various gaseous elements is represented for two secondary dendrite arm spacings, with and without shrinkage. It can be seen that dissolved H_2, H_2O and SO_2 can have a concomitant effect on the microporosity level. The selected oxygen nominal concentration is low (20 ppm (at)) in order to avoid Cu_2O precipitation in the liquid phase (see Cu-O phase diagram), a situation that the model is unable to handle if X^l_O path is unknown. The chosen sulphur nominal concentration is high (0.8 % (at)), i.e., at least twice the concentration usually added to improve machinability. It is observed that the presence of hydrogen creates a significant amount of porosity (diamonds), but this amount is drastically increased with the presence of oxygen (formation of water vapour). This figure also shows that the presence of sulphur can produce porosity if no deoxidation step was employed before pouring.

In Fig. 4, the porosity fraction is represented as a function of hydrogen and oxygen nominal concentrations for different secondary dendrite arm spacings, without and with account of solidification shrinkage, using the thermal gradient and isotherm speed mentioned before. Several thousand computations were made, but the presence of sulphur was not considered. In Figs 4(a) and (b), it is observed that, at high O and H nominal concentrations, the porosity fraction slightly decreases with the secondary dendrite arm spacing. At low gaseous element concentrations, the porosity level is larger for smaller λ_2 values because the permeability is reduced [19] (i.e., the pressure drop is larger). This effect is apparently larger than the opposite one associated with the curvature contribution (i.e., higher Δp_r with smaller λ_2). On the other hand, solidification shrinkage has a strong influence on the porosity level. This is confirmed in Fig. 4: (i) for high nominal concentrations of gaseous elements, the porosity fraction is significantly lower when the shrinkage is not account for, and (ii) the porosity fraction is zero at low gaseous element concentrations, whereas it is not zero when shrinkage is accounted for. These maps would allow the determination of the gaseous element nominal concentrations below

which the porosity fraction will be lower than a given value. Of course, these concentrations strongly depend on the process and alloy parameters.

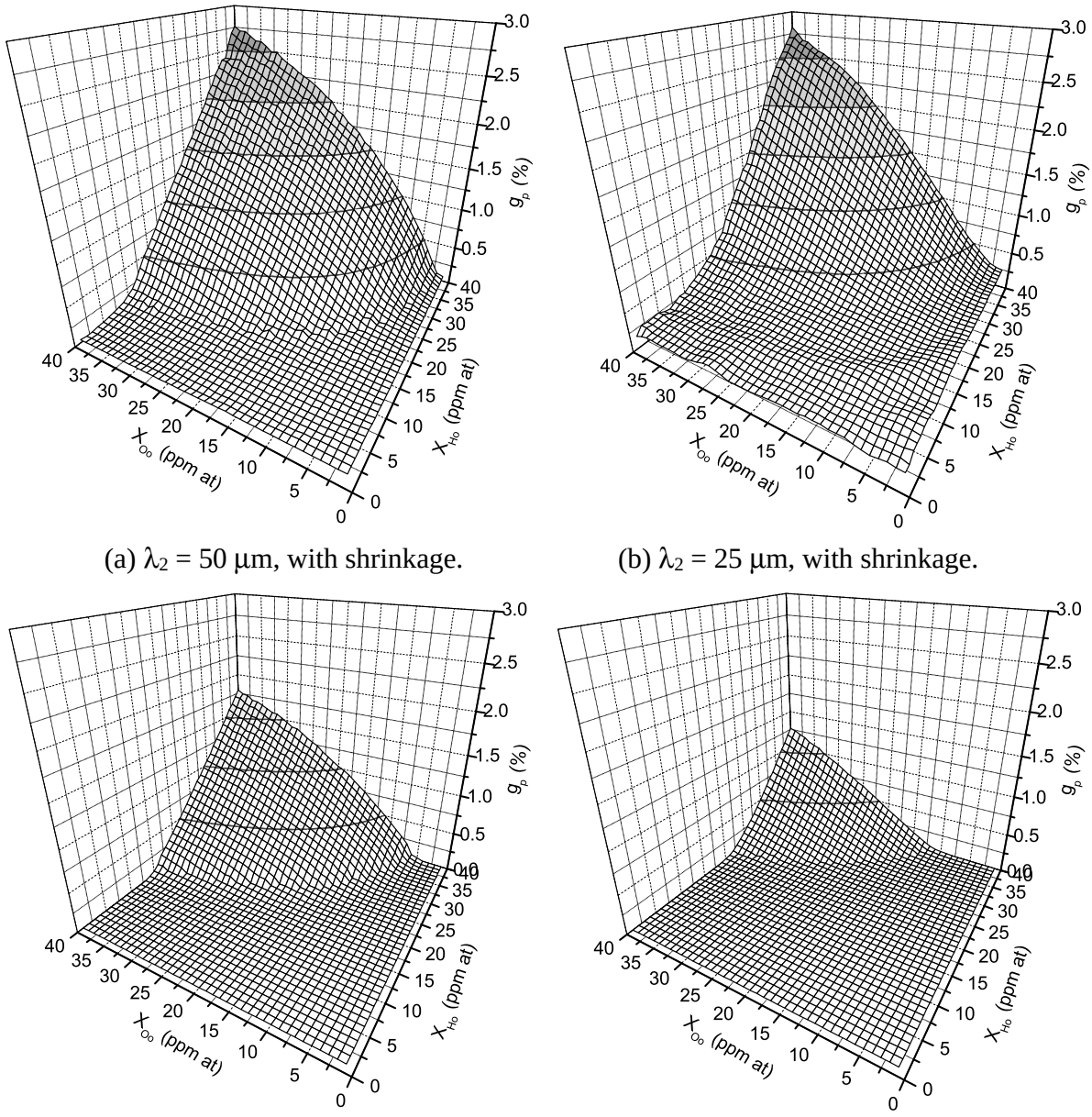

(a) λ_2 = 50 μm, with shrinkage.

(b) λ_2 = 25 μm, with shrinkage.

(c) λ_2 = 50 μm, without shrinkage .

(d) λ_2 = 25 μm, without shrinkage.

Figure 4. Maps of the porosity fraction in Cu-10wt%Zn as a function of H and O nominal concentration and for different secondary dendrite arm spacings, without and with account of solidification shrinkage.

Conclusion

In this paper a general approach to model porosity in multi-component alloys for multi-gas systems has been detailed. An application to Cu-Zn has shown the influence of various gas elements, of the secondary dendrite arm spacing and of solidification shrinkage. The contribution of the vapour pressure of volatile solute elements such as zinc is detailed elsewhere [17]. This model is being validated on several aluminium alloys.

Acknowledgements

The authors would like to thank the financial support of the Commission for Innovation and Technology, CTI, Bern (grant 6167.1 KTS), and of the industries Alcan (CH), Alcan (FR), Calcom-ESI (CH), HydroAluminium (DE), General Motors (USA) and Union Minière (BE).

References

1. Ch. Pequet, M. Gremaud, and M. Rappaz, "Modelling of microporosity, macroporosity, and pipe-phrinkage formation during the solidification of alloys using a mushy-zone refinement method: applications to aluminium alloys", *Met. Mater. Trans.*, **33A** (2002) 2095.
2. M.J. Couper, A.E. Neeson, and J.R. Griffiths, "Casting defects and the fatigue life of an aluminum casting alloy". *Fatigue Fract. Eng. Mater. Struct*., **13** (1990) 213.
3. B. Skallerud, T. Iveland, and G. Härkegård, "Fatigue life assessment of aluminum alloys with casting defects", *Eng. Fracture Mech.*, **44** (1993) 857.
4. Q.G. Wang, D. Apelian, and D.A. Lados, "Fatigue behaviour of A356-T6 aluminum cast alloys. Part I. Effect of casting defects", *Journal of Light Metals*, **1** (2001) 73.
5. M. Garat, "Effets respectifs de la finesse de structure et de la compacité sur les caractéristiques mécaniques statiques et dynamiques de l'A-S7G06", *Fonderie Fondeurs d'aujourd'hui*, **nov.** (1989) 21.
6. M. Morishita, K. Nakayama, and M.G. Chu, "Effect of Hydrogen Porosity and As-Cast Grain Structure on the Mechanical Properties of Cast and Forged Al-1.0Mg-0.6Si Alloy", *Solidification Of Aluminum Alloys*, Eds Men G. Chu et al (TMS Pub., Warrendale, USA, 2004) p. 283.
7. H. Darcy, (1856), *Les Fontaines Publiques* (Dalmont Publ., France).
8. J. Campbell, *Castings* (Elsevier, 2003).
9. *Smithells Metals Reference Book*, 7th edition, Eds E.A. Brandes and G.B. Brook (Butterworth-Heinemann Publ., Woburn, MA, USA, 1992).
10. J. Charbonnier, "Gaz dans les alliages d'aluminium de fonderie", *Traité Matériaux Métalliques*, (Techniques de l'Ingénieur, 1991) article M218.
11. G. K. Sigworth, and T. A. Engh, "Chemical and kinetic factors related to hydrogen removal from aluminium." *Met. Mater. Trans.*, **13B** (1982) 447.
12. *Series on the metallurgy of copper*, (The International Copper Research Association, Library of Congress, USA, 1977).
13. *ASM Casting Handbook*, Vol. **15**, 4th edition, Ed. D.M. Stefanescu et al (ASM Intern., Metals Park, Ohio, USA, 1998).
14. P.K. Sung, D.R. Poirier, and S.D. Felicelli, "Continuum model for predicting microporosity in steel castings", *Modelling Simul. Mater. Sci. Eng.*, **10** (2002) 551.
15. D.R. Poirier, M.M. Andrews, and A.L. Maples, "Modeling macrosegregation and porosity in steel castings", *1st International Steel Foundry Congress* (Steels Founders' Society of America, Des plaines, IL, USA, 1985), 307.
16. J. Philibert, A. Vignes, Y. Bréchet, and P. Combrade, *Métallurgie du minerai au matériau* (Masson, Paris, 1998).
17. G. Couturier, and M. Rappaz, "Effect of volatile elements on porosity formation in solidifying alloys", *Modelling Simul. Mater. Sci. Eng.*, (2005) to appear.
18. Landolt-Bornstein, *Phase equilibria, crytallographic and thermodynamic data of binary alloys*, New series, group IV, macroscopic properties of matter, (Springer Verlag, 1994).
19. D. R. Poirier, "Permeability for flow of interdendritic liquid in columnar-dendritic alloys", *Met. Mater. Trans.* **18B** (1987) 245.